Importance of Nonlinear Wave Representation for Nonlinear Froude-Krylov Force Calculations for Wave Energy Devices

Giuseppe Giorgi
Centre for Ocean Energy Research, Maynooth University
Co.Kildare, Ireland
E-mail: giuseppe.giorgi.2015@mumail.ie

John V. Ringwood
Centre for Ocean Energy Research, Maynooth University
Co.Kildare, Ireland
E-mail: john.ringwood@nuim.ie

***Abstract*—Due to their computational convenience, mathematical models for wave energy converters are usually linear. Including nonlinearities may improve the accuracy of the results, but often at the price of an additional computational and complexity burden, which can be justified only if nonlinearities are significant.**

One of the sources of nonlinearity in fluid-body interactions is the wave field itself. Different wave models exist, among which are linear Airy's theory, the Wheeler stretching approach, and the nonlinear Rienecker-Fenton method, which achieve a different compromise of accuracy and complexity.

The impact of the accuracy of such wave theories strongly depends on the specific device (operating principle, power production region and survivability mode), and installation site (water depth, occurrences of each sea state in the scatter diagram of the installation site). This paper evaluates the performance of different wave field representations, firstly in absolute terms, and secondly in relation to the associated computation of nonlinear Froude-Krylov forces for different wave energy devices.

***Index Terms*—Nonlinear wave, Wheeler stretching, Rienecker-Fenton wave, nonlinear Froude-Krylov force, wave energy converters.**

I. Introduction

Linear mathematical models are commonly used to describe wave energy converters (WECs) dynamics, since they have the advantage of being very computationally efficient. Nonetheless, including nonlinear effects may improve the accuracy of the model, but often at the cost of an additional computational and complexity burden, which can be justified only if nonlinearities are significant.

Nonlinearities in fluid-body interactions depend on:

(i) The free surface elevation
(ii) The pressure field distribution
(iii) Geometrical nonlinearities

Points i) and ii) concern the modelling of the wave field, which is the energy source, while point iii) concern the computation of the hydrodynamic forces acting on the body, which are defined as the integral of the pressure acting on the wetted surface of the device. In particular, Froude-Krylov (FK) forces are the hydrodynamic components which describe the action of the undisturbed incident wave on a device; therefore, accurate modelling of FK forces is likely to be important for simulating reliable responses of heaving WEC devices, which are excited mainly by FK forces, while surge devices are equally responsive to diffraction and FK forces, as shown in [1]. For example, [2] show that geometrical nonlinearities may be relevant for the FK force calculation for heaving point absorbers (HPAs), significantly affecting the response of the device.

Including geometrical nonlinearities for the computation of nonlinear FK forces implies an increase in complexity and computational time, which depends on the complexity of the geometry itself: for relatively simple geometries, as axisymmetric heaving point absorbers or oscillating wave surge converters (OWSCs), computationally-efficient algebraic solutions are available [3], while complex geometries require more complex approaches [4].

Likewise, different degrees of accuracy (at different complexity costs) can be achieved in modelling the incident wave field, starting from the most simple linear Airy theory, to several nonlinear wave formulations, including Stokes' waves (2nd to 4th order), cnoidal waves, and Rienecker-Fenton (RF) waves [5]. Finally, corrections to linear theory, such as Wheeler's stretching method [6], can be used to improve the results of Airy's theory, at a negligible additional complexity cost. The accuracy of such wave theories depends mainly on the water depth and the wave steepness; therefore, the impact of such nonlinearity strongly depends on the specific device (position of the device with respect to the free surface and the sea bottom; power production region and survivability mode), and installation site (water depth; occurrence of each sea state in the scatter diagram of the installation site).

This paper discusses the impact that the choice of the wave field representation model has on the accuracy and complexity of the calculation of FK forces for wave energy devices. Linear Airy's theory, Wheeler stretching and nonlinear Rienecker-Fenton waves are considered: firstly, the pressure profile is evaluated and compared, from the free surface to the sea bottom, for a comprehensive set of wave conditions. Secondly, the effect of different pressure field representations on the calculation of FK forces for WECs is discussed, considering HPAs and OWSCs as representative devices.

The reminder of the paper is organized as follows: Sect. II presents the wave models, based on potential theory. Sect. III evaluates the overall accuracy of the pressure profile representation, while Sect. IV takes into account the effect of the pressure representation in the context of nonlinear modelling for wave energy devices. Some final remarks and conclusions are presented in Sect. V.

II. Wave theories

The wave theories discussed herein are based on the assumption of a homogeneous, ideal, incompressible fluid, with irrotational motion [7]. Two-dimensional waves are considered in the (x, z) coordinate system, where x is the direction of propagation of the wave, and z is the vertical axis, positive upwards, with origin at the still water level (SWL), which is at a distance d from the sea bed. Assuming fluid incompressibility, a velocity potential φ can be defined, such that:

$$\mathbf{u} = \nabla\varphi \tag{1}$$

where $\mathbf{u}$ is the velocity vector. Since the motion is assumed irrotational, φ satisfies the Laplace's equation throughout the fluid:

$$\nabla \times \mathbf{u} = \nabla^2\varphi = 0 \tag{2}$$

The periodic boundary condition is satisfied on the lateral boundaries, with spacial period equal to the wave length λ. The kinematic boundary conditions are satisfied on the sea bottom, (3a), and on the free surface η, (3b):

$$\frac{\partial\varphi}{\partial z} = 0, \qquad \text{at } z = -d \tag{3a}$$

$$\frac{\partial\varphi}{\partial z} = \frac{\partial\eta}{\partial t} + \frac{\partial\varphi}{\partial x}\frac{\partial\eta}{\partial x}, \qquad \text{at } z = \eta \tag{3b}$$

Finally, the dynamic boundary condition (Bernoulli's equation) is verified on the free surface:

$$\frac{\partial\varphi}{\partial t} + \frac{p_{dy}}{\rho} + gz + \frac{|\nabla\varphi|^2}{2} = 0, \qquad \text{at } z = \eta, \tag{4}$$

where ρ is the water density, g the acceleration of gravity, and p_{dy} the dynamic pressure. The static pressure is defined as $p_{st} = -\rho g z$.

A general analytical solution for the wave potential problem, described by equations (1) to (4), does not exist. In particular, some further assumption are needed to solve the free surface boundary conditions (3b) and (4): Airy's wave theory linearizes such boundary conditions onto the SWL, while Stokes' wave theory, assuming infinite water depth (with respect to λ), uses a Fourier series of (3b) and (4), performing a perturbation expansion in terms of a small parameter, which increases with the wave height; on the other hand, cnoidal wave theory solves the potential problem assuming that the wave length is much longer than the water depth.

The regions of validity of such wave theories are shown in Fig. 1. Note that there are different orders of Stokes' theory, where the first order on the bottom, not explicitly labelled in Fig. 1 for lack of space, corresponds to the linear Airy's theory. The range of applicability of the different theories is defined by the water depth, the wave length and the wave height H. The limit between shallow and infinite water depth is given by an Ursell number (Ur) equal to 40 [8], where Ur is the ratio between a measure of nonlinearity (H/d), and a measure of shallowness (d^2/λ^2). The theoretical limit for the highest wave possible, based on [9], determines the maximum achievable wave height, after which the wave breaks and the potential theory is no longer applicable.

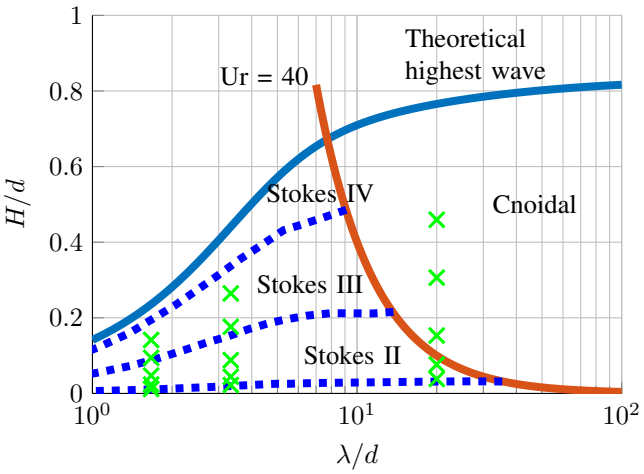

Fig. 1: Regions of validity of wave theories for different wave lengths λ and wave height H, both normalized with respect to the water depth d. The limit between shallow and infinite water depth is given by the Ursell number (Ur) equal to 40 [8]. The theoretical highest wave possible is based on [9]. The markers on the graph refer to the wave conditions studied in Section III

Finally, by means of the Rienecker-Fenton wave's theory [5], it is possible to achieve a numerical solution of the nonlinear potential problem, without any assumption on the wave depth or height. Indeed, [10] shows how well RF waves embraces Stokes' and cnoidal wave theory, in the respective regions of validity, which have been widely validated against experimental tests [11]. The drawback is that, while there are analytical formulations for calculating the Stokes' and cnoidal waves parameters, RF approach requires a numerical optimization routine for each wave condition.

A. Linear Airy's wave theory

Assuming a small wave steepness ($s = H/\lambda$), it is possible to linearize the kinematic and the dynamic free surface boundary conditions, shown in (3b) and (4), respectively, around the SWL, namely at $z = 0$. The solution of the linearized potential problem consists of a harmonic free surface elevation and an exponential dynamic pressure, as follows:

$$\eta = \frac{H}{2}\cos\left(kx - \omega t\right) \tag{5a}$$

$$p_{dy} = \rho g \eta \frac{\cosh k\left(z+d\right)}{\cosh kd} \tag{5b}$$

where $k = 2\pi/\lambda$ is the wave number, $\omega = 2\pi/T$ is the wave frequency, and T the wave period. Note that, at infinite water depth conditions, the dynamic pressure tends to $\rho g \eta e^{k\eta}$.

At the free surface ($z = \eta$), the total pressure p should match the atmospheric pressure, equal to zero. According to Airy's wave theory at infinite water depth, p at the free surface is given as:

$$p = p_{st} + p_{dy} = -\rho g \eta + \rho g \eta e^{k\eta} = \rho g \eta \left(e^{k\eta} - 1\right) \tag{6}$$

As a consequence of the linearization of the free surface boundary conditions, the total pressure is zero at the SWL ($z = 0$) instead, implying a modelling error of the pressure at the actual free surface. Equation (6) shows that such an error is proportional to $\left(e^{k\eta} - 1\right)$, which tends to zero as the wave steepness tends to zero.

B. Wheeler's stretching method

The Wheeler stretching approach [6] consists of starting from the results obtained with the Airy's theory, and apply a convenient change of coordinates, in order to correct the free surface boundary condition error: the vertical coordinate z is substituted with z', defined as:

$$z' = d\frac{z+d}{\eta+d} - d \tag{7}$$

Note that the origin of the stretching is located at the sea bottom, since $z' = z$ at $z = -d$. On the other hand, $z' = 0$ at $z = \eta$, hence the free surface boundary condition is satisfied. Notwithstanding the dynamic pressure is punctually correct at $z = \eta$, the whole pressure profile is, in general, an approximation, since it is based on a linear stretching of the results from the Airy's theory.

C. Rienecker-Fenton wave theory

The basis of the Rienecker-Fenton method is to write the analytical solution for φ in a separated variables form:

$$\varphi = \sqrt{\frac{g}{k^3}} \sum_{j=1}^{N_B} B_j \frac{\cosh jk(z-d)}{\cosh jkd} \sin jkx \tag{8}$$

where B_j are dimensionless constants for a particular wave, and N_B is a finite integer which, according to [5], should be chosen between 10 and 20. The truncation of the series for finite N_B is the only approximation in this formulation. The values of B_j are found numerically, using Newton's method [5].

Note that the complexity of the pressure formulation in the RF method is considerably higher than in Airy's theory and Wheeler's stretching method. In fact, once the N_B terms of the potential are obtained, the pressure is computed from Bernoulli's equation (4), which requires the computation of derivatives of the potential. On the other hand, since no approximation is introduced in the boundary condition formulation, the wave pressure profile obtained with the RF method is taken as an accuracy benchmark, and used to evaluate Airy and Wheeler approaches. Likewise, the RF approach provides an accurate description of the nonlinear free surface elevation, with higher and steeper peaks with respect to linear waves. Fig. 2 shows an example of free surface elevation, using Airy's theory and the RF model.

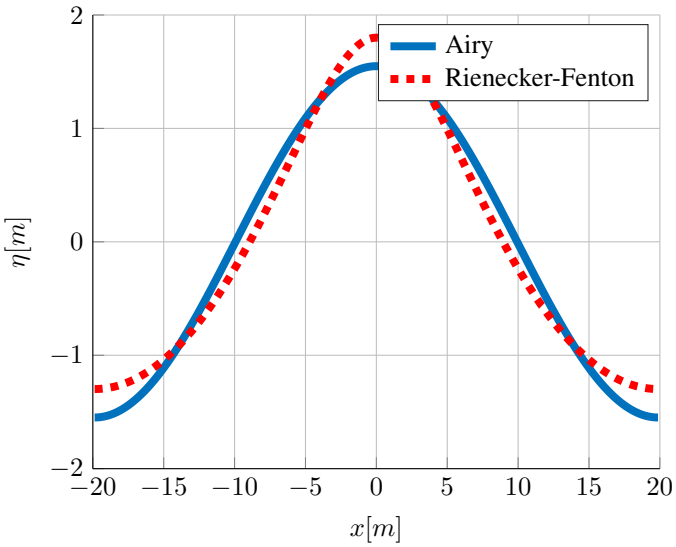

Fig. 2: Free surface elevation for a wave condition with $T = 5s$, $H = 3m$, $d = 12m$, using Airy's theory, equation (5a), and Rienecker-Fenton theory, derived from equation (8) [5].

III. Pressure Profile

The objective of the study is to evaluate the influence of nonlinear waves on nonlinear FK forces for wave energy converters. The two elements affecting the response of the device are the free surface elevation and the pressure profile. On the one hand, η is just an input to the system, therefore its complexity does not affect the complexity of the WEC model, since η is evaluated only once. On the other hand, the pressure profile has to be evaluated, and integrated over the wetted surface of the device, at each time step; therefore, the computational burden of the calculation of nonlinear FK forces is strongly dependent on the complexity of the pressure formulation, while independent of η. Hence, hereafter the nonlinear η is considered for all wave models.

The shape of the pressure profile is evaluated for a comprehensive range of wave conditions. Three wave periods are considered, equal to 5s, 10s, and 15s, and the corresponding wave lengths are computed according to the water waves dispersion relation [12]. Three normalized water depths d/λ are considered, equal to 0.05, 0.3 and 0.6, respectively defining shallow, intermediate and infinite water depth conditions [12].

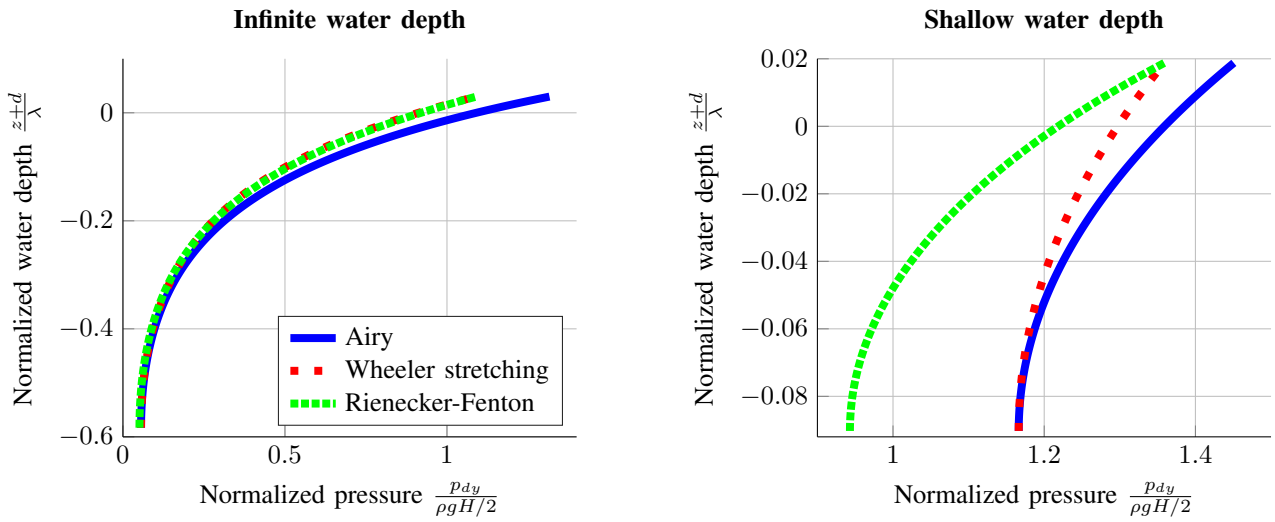

Fig. 3: Normalized pressure profiles for infinite and shallow water depth conditions, for a wave sample with wave height equal to 40% of the theoretical maximum wave height. The corresponding wave steepness are 2.8% in shallow water depths, 5.5% in infinite water depth.

Finally, for each wave condition, five wave heights are studied, corresponding to 5%, 10%, 20%, 40%, and 60% of the theoretical maximum wave height, as defined in [9]. The resulting waves conditions are shown by the markers in Fig. 1.

It is worth to highlight that the wave period has just the effect of scaling the free surface elevation and pressure profiles, changing the wave length; therefore, the markers in Fig. 1 overlap for different T. Likewise, the normalized pressure profiles for different T, but same λ/d and H/d, overlap.

Fig. 3 shows two representative samples of pressure profiles, at the wave peak ($z = \eta$), having the wave height equal to 40% of the theoretical maximum wave height. In infinite water depth conditions, RF pressure profile significantly differs from Airy's one only at the free surface, converging to almost the same value at the sea bottom, where the dynamic pressure is almost zero, due to the large distance between the wave and the sea bed. Conversely, large errors are found in shallow water conditions, throughout the whole water depth, since the nonlinear influence of the near sea bed is considerably changing the pressure decay rate from the free surface to the bottom.

The Wheeler stretching approach, as explained in Sect. II-B, analytically imposes the correct boundary condition at the free surface, and linearly stretches the pressure profile from the sea bottom. Indeed, Fig. 3 shows that the pressure according to the Wheeler stretching model is the same as the RF's one at the free surface, while is the same as the Airy's one at the sea bottom. Consequently, errors in the pressure profile modelling for the Wheeler stretching approach are dependent on the pressure errors at the sea bottom, which increase with the shallowness of the wave.

In order to have a more global picture of the errors committed by Airy's theory and the Wheeler stretching model, compared to the RF benchmark model, the mean relative error is computed for all the wave conditions shown in Fig. 1. The relative pressure difference is evaluated at N vertical points, from the sea bottom to the peak free surface. Given the variety of water depths considered, trying to define a depth-independent error index, the same number of points is taken for all the waves. On the other hand, since the pressure decay close to the free surface is faster than in deeper water, with a characteristic exponential decay, the N points are chosen with a logarithmic spacing, so that points are denser close to the free surface, and looser towards the sea bed. Fig. 4 plots such relative errors against the wave steepness, which is a representative parameter of the degree of nonlinearity in the wave, as discussed in Sect. II. Finally, note that a positive relative error stands for an overestimation of the pressure.

In general, Fig. 4 shows that the relative error is always increasing with the wave steepness, namely with the amount of nonlinearity in the wave. Besides, for linear waves (steepness lower than 1%), the relative error is lower than 2% for both models, in all depth conditions. On the other hand, as the steepness increases, the curves diverges and the relative error obtained using Airy's theory reaches a maximum of 28%, while with the Wheeler stretching approach, the maximum error is less than 2% in intermediate/infinite water depths, about 8% in shallow water conditions. It is evident that the Wheeler stretching model always outperforms the Airy's theory: as expected, drastic improvement is found at intermediate and infinite water depth conditions, where the relative errors are between 12 and 23 times smaller while, at shallow water depth, the relative error is about half.

IV. Pressure Integral

The errors shown in Fig. 4 give an *overall* evaluation of the pressure profile representation, from the sea bottom to the free surface, according to the Airy's and Wheeler stretching approaches. Nevertheless, as far as nonlinear modelling of wave energy converters is concerned, what is important is the

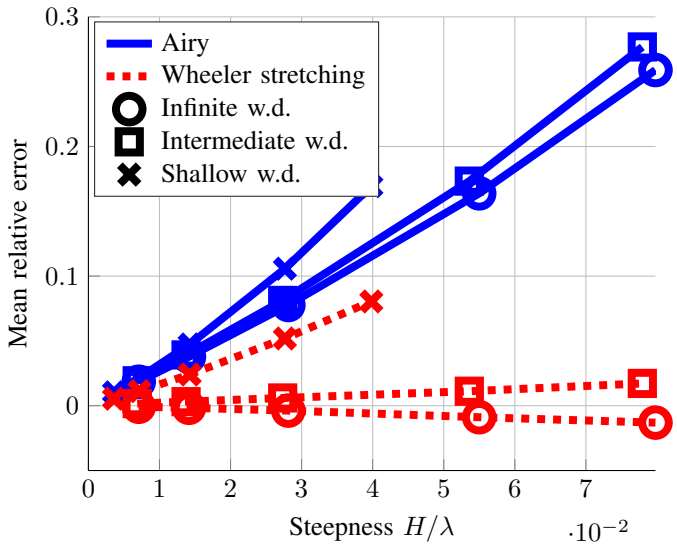

Fig. 4: Relative error committed by Airy's theory (in blue) and the Wheeler stretching (in red) model, compared to the RF benchmark model, for the three water depth (w.d.) conditions, which are represented by the black markers in the legend. In the plot, markers have the same colour of the wave theory.

accuracy just in the region of fluid where the device operates, which affects the accuracy of the computation of the nonlinear Froude-Krylov force.

Consequently, the device operating principle has to be taken into account. On the one hand, surface piercing heaving point absorbers are considered, which work in the proximity of the free surface, in either infinite or intermediate water depth conditions. On the other hand, oscillating wave surge converters are studied, which operate in intermediate/shallow water conditions, spanning almost all the depth from the free surface to the sea bed. Therefore, based on Figs. 3 and 4, it can be expected that the Wheeler stretching approach can be more effective for HPAs than for OWSCs, since the Wheeler stretching errors are particularly small close to the surface, and in infinite or intermediate water conditions.

Inspired by the Wavestar device [13], a spherical HPA is chosen, with radius of 2.5m, and centre at the still water level. The dynamic nonlinear FK force is the integral of the dynamic pressure over the instantaneous wetted surface, which depends on the relative displacement between the device and the free surface elevation. The details for an algebraic resolution of such an integral are given in [14]. Besides, the geometry of the OWSC is based on the Oyster 2 device [15]. The dynamic FK torque is the resulting torque due to the pressure on the front and rear surfaces of the flap, as shown in [3].

The reason for considering the device geometry is to quantify the importance of the nonlinear pressure profile in the respective operating region. Therefore, with the purpose of excluding geometrical nonlinearities, a zero relative displacement is used for the HPA, and the vertical (rest) position is considered for the OWSC. Therefore, the HPA is modelled as half a sphere, with radius 2.5m, while the OWSC is modelled as a rectangle, with 9m draft and 26m width. The dynamic pressure is consequently integrated over the two geometries to calculate FK forces.

Fig. 4 shows how modelling errors significantly increase with the wave steepness. However, the occurrence of highly nonlinear waves is likely to be low, therefore the scatter diagram of the installation site has to be considered as well. Furthermore, the device is designed to be operative only in a determined range of wave conditions, where the physical constraints are respected, and the power absorption is guaranteed. Otherwise, for certain wave conditions, the device is not able to produce energy (if the waves are not energetic enough), or it turns into survivability mode (if the waves are too energetic).

Therefore, for power production assessment studies, the accuracy of the wave representation is important only in the power production region. On the contrary, highly nonlinear and energetic sea states must be considered when the maximum structural loads need to be assessed. However, more complex fully nonlinear models, like computational fluid dynamics (CFD), are likely to be necessary for such survivability studies.

The scatter diagram considered in this study is shown in Fig. 5, which refers to the European Marine Energy Centre (EMEC), Orkney, Scotland [16]. The solid line defines the operational region of the OWSC Oyster800, which covers the 86.1% of the total wave occurrences.

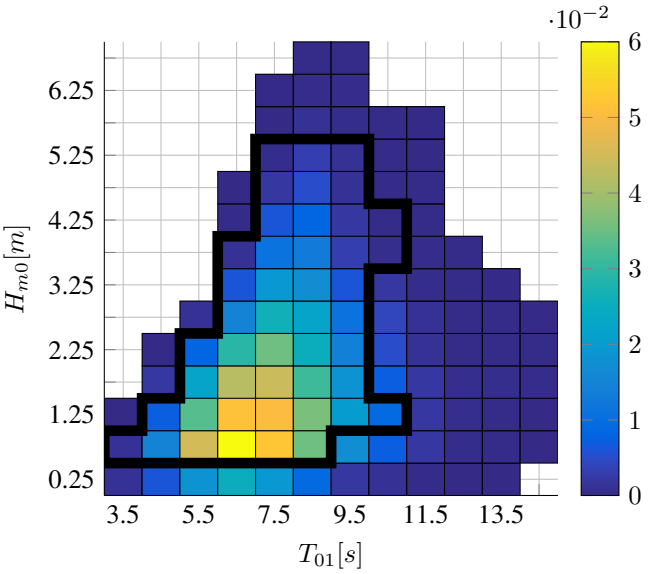

Fig. 5: Significant wave height H_{m0}, mean wave period T_{01} scatter diagram at the European Marine Energy Centre (EMEC), Orkney, Scotland. The solid line defines the operational region of the OWSC Oyster800, which covers 86.1% of the total wave occurrences [16].

A set of regular wave conditions is based on the significant wave heights (H_{m0}) and mean wave periods (T_{01}) shown in Fig. 5. The water depth choice, equal to 13m, is constrained by the OWSC geometry [15]. However, the HPA is studied in infinite water depth conditions as well.

Integrals of the dynamic pressure over the surface of the HPA and the OWSC are computed at the peak of the free surface elevation, in order to highlight nonlinear effects. The computation of such nonlinear integrals is straightforward for the Airy's pressure profile, since algebraic solutions are available, in [14] for the HPA, in [3] for the OWSC. The very same algebraic solution can be easily adapted to the Wheeler stretching pressure profile, since just a change of variable is required. On the contrary, integrating the RF pressure profile is much more complex: given the high number of terms of the RF pressure expression, an algebraic solution does not exist, and a numerical integration scheme must be used. It results that the numerical integration scheme for the RF approach is about two orders of magnitude slower than the algebraic solution, which is applicable only to linear and Wheeler stretching approaches.

As in Sect. III, the results obtained using the RF model are used as benchmark to evaluate Airy's and Wheeler stretching models, whose relative errors are shown in Figs. 6 and 7, for the HPA and the OWSC, respectively. In both figures, the surface on the top refers to the Airy's model, whereas the surface on the bottom refers to the Wheeler stretching approach, whose errors are indeed always smaller.

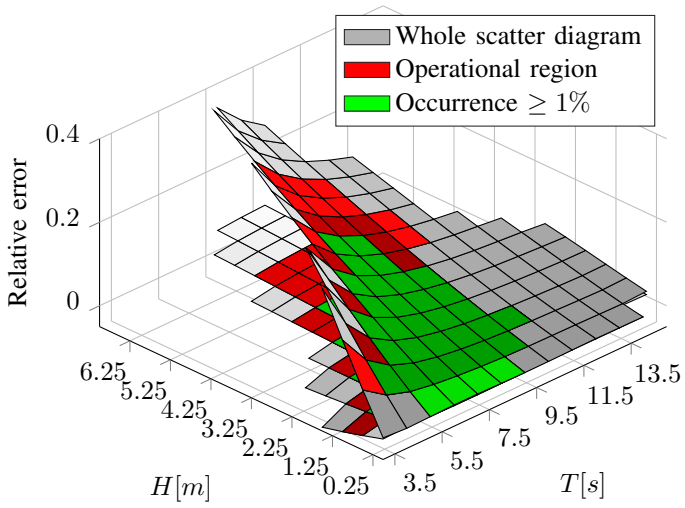

Fig. 6: Relative error in the pressure integral for the HPA (water depth of 13 m), using the Airy's pressure (on the top), and the Wheeler stretching pressure (on the bottom).

Each surface in Figs. 6 and 7 presents three different shades (grey, red, and green). The first and outer one covers the whole scatter diagram. The second shade considers only the wave conditions within the operational region of the scatter diagram, shown in Fig. 5, which is the region of interest for power production assessment studies. The third and inner shade takes into account only the wave conditions which pass a significant occurrence threshold, arbitrary set at 1%. Indeed, higher accuracy is required in more probable wave conditions, while larger errors can be accepted for rare wave conditions. The sum of the occurrences over 1% amount to 87%, which is comparable to the 86.1% of the whole operational region.

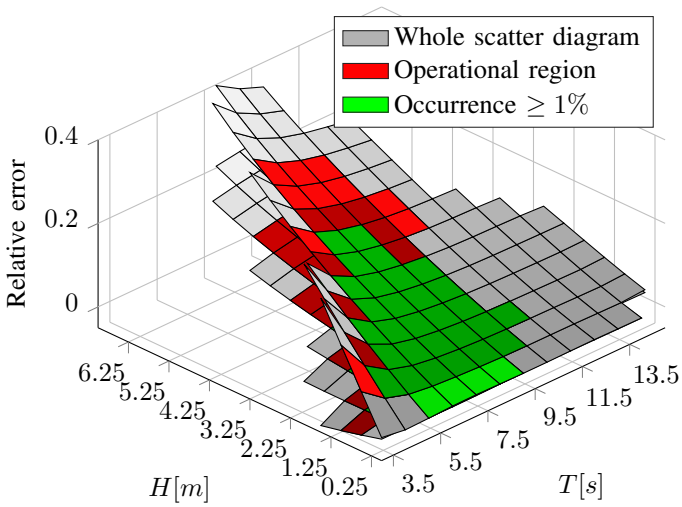

Fig. 7: Relative error in the pressure integral for the OWSC, using the Airy's pressure (on the top), and the Wheeler stretching pressure (on the bottom).

Using Airy's theory leads to produce similar errors in both the HPA and the OWSC, up to 36% in the full scatter diagram, up to 28 % in the operational region, and up to 18% in the occurrence threshold region. Conversely, the Wheeler stretching method performs better for the HPA than the OWSC, with maximum errors of 5% and 20%, respectively. Indeed, HPAs work close to the free surface, where the boundary condition error is zero, thanks to the Wheeler stretching change of coordinates.

Finally, the HPA is studied in infinite water condition as well. Smaller errors are found, with respect to the 13 m water depth condition: Airy's theory maximum error drops from 32% to 25%, while Wheeler stretching maximum error drops from 5% to 4%. A summary of the maximum errors in each of the three regions (whole scatter diagram, operational region, and occurrence threshold region) is tabulated in Table I.

V. Conclusion

The accuracy of nonlinear hydrodynamic models for wave energy converters is directly influenced by the fidelity of the wave field representation. Concurrently, accuracy improvements have to be weighted by the increase in complexity and computational cost, required to implement more accurate wave models. This paper considers three different modelling approaches, namely the linear Airy's theory, the Wheeler stretching approach and the Rienecker-Fenton method. Fig. 4 shows how the Wheeler stretching method performs always better than the Airy's theory, especially in infinite/intermediate water depth conditions, achieving a maximum relative error less than 2% in intermediate water depth, less than 8% in shallow water depth. Nevertheless, the complexity of the Wheeler stretching approach is the same as the Airy's one, but much simpler than the RF one.

As far as WEC nonlinear models are concerned, only the region of fluid where the device operates is relevant for the

TABLE I: Maximum errors for the whole scatter diagram, the operational region, and occurrence threshold region, for the HPA and the OWSC. The subscript indicates the water depth for each of the device.

		HPA_∞		HPA_{13}		$OWSC_{13}$	
		Airy	Wheeler stretching	Airy	Wheeler stretching	Airy	Wheeler stretching
Occurrence $\geq 1\%$	(total 87%)	14.1%	-1.0 %	17.3 %	3.1%	18.2 %	9.1 %
Operational boundary	(total 86.1%)	20.6 %	-2.4 %	26.0 %	4.4 %	27.8 %	14.7 %
Whole scatter diagram	(total 100%)	25.1 %	-4.2 %	32.5 %	5.3 %	35.8 %	20.5 %

final accuracy of the results. Indeed, Figs. 6 and 7 show that the Wheeler stretching method performs better than the Airy's theory, but produces much smaller errors in HPAs with respect to OWSCs.

Furthermore, it is important to highlight that the performance of the wave models have to be weighted with the occurrence of each sea condition, according to the scatter diagram of the installation site. An other criterion to consider is the operational region, which is the only one taken into account for power production assessment studies. Table I shows that the maximum errors in different areas of the scatter diagram may vary significantly.

Finally, it can be concluded that the Wheeler stretching approach is a convenient wave modelling option, since it performs well compared to the RF method, especially for HPAs, and performs always better than the Airy's theory, but maintaining the same level of complexity.

ACKNOWLEDGMENT

This paper is based upon work supported by Science Foundation Ireland under Grant No. 13/IA/1886.

REFERENCES

[1] G. Giorgi and J. V. Ringwood, "Comparing nonlinear hydrodynamic forces in heaving point absorbers and oscillating wave surge converters," *submitted to Journal of Ocean Engineering and Marine Energy*, 2017.

[2] G. Giorgi, M. Penalba, and J. V. Ringwood, "Nonlinear hydrodynamic models for heaving buoy wave energy converters," in *Proceedings of the 3rd Asian Wave and Tidal Energy Conference*, 24-28 October 2016, pp. 144–153.

[3] ——, "Nonlinear hydrodynamic force relevance for different wave energy converter types," in *Proceedings of the 3rd Asian Wave and Tidal Energy Conference*, 24-28 October 2016, pp. 154–162.

[4] J.-C. Gilloteaux, "Mouvements de grande amplitude d'un corps flottant en fluide parfait. application à la récupération de l'énergie des vagues." Ph.D. dissertation, Ecole Centrale de Nantes-ECN, 2007.

[5] J. Fenton, "Nonlinear wave theories," *the Sea*, vol. 9, no. Part A, pp. 3–25, 1990.

[6] J. Wheeler, "Methods for calculating forces produced on piles in irregular waves," *Journal of Petroleum Technology*, no. 249, pp. 359–367, 1970.

[7] J. Newman, *Marine Hydrodynamics*. MIT Press, 1977.

[8] T. Hedges, "Regions of validity of analytical wave theories," in *ICE Proceedings Water Maritime and Energy*, vol. 112, no. 2, Janvier 1995, pp. 111–114.

[9] J. Williams, "Limiting gravity waves in water of finite depth," *Philosophical Transactions of the Royal Society of London A: Mathematical, Physical and Engineering Sciences*, vol. 302, no. 1466, pp. 139–188, 1981.

[10] R. J. Sobey, P. Goodwin, R. J. Thieke, and R. J. Westberg Jr, "Application of stokes, cnoidal, and fourier wave theories," *Journal of waterway, port, coastal, and ocean engineering*, vol. 113, no. 6, pp. 565–587, 1987.

[11] B. Le Mehaute, D. Divoky, and A. Lin, "Shallow water waves a comparison of theories and experiments," in *Coastal Engineering 1968*, 1969, pp. 86–107.

[12] R. G. Dean and R. A. Dalrymple, *Water wave mechanics for engineers and scientists*. World Scientific Publishing Co Inc, 1991, vol. 2.

[13] Wavestar, "Wavestar a/s, available at http://wavestarenergy.com/," 2016.

[14] G. Giorgi and J. V. Ringwood, "Computationally efficient nonlinear froude–krylov force calculations for heaving axisymmetric wave energy point absorbers," *Journal of Ocean Engineering and Marine Energy*, pp. 1–13, 2016.

[15] Aquamarine, "Aquamarine power, available at http://http://www.aquamarinepower.com/," 2016.

[16] L. O'Boyle, K. Doherty, J. van't Hoff, and J. Skelton, "The value of full scale prototype data-testing oyster 800 at emec, orkney," in *Proceedings of the 11th European Wave and Tidal Energy Conference (EWTEC), Nantes, France*, 2015, pp. 6–11.